*H2020-FETOPEN-2019-01*

*FET-Open Challenging Current Thinking*

# POSEIDON

**NanoPhOtonic devices applying Self-assembled colloIDs for novel ON-chip light**

Starting date of the project: 01/01/2020
Duration: 48 months

# = Deliverable D3.3 =

## Report on targeted on-chip deposition of colloid light source

Due date of deliverable: 31/12/2023
Actual submission date: 17/01/2024

WP and Lead Beneficiary: WP3, FAU
Version: V1.0

| **Dissemination level** | | |
|---|---|---|
| PU | Public | x |
| CO | Confidential, only for members of the consortium (including the Commission Services) | |
| CI | Classified, information as referred to in Commission Decision 2001/844/EC | |

This project has received funding from the European Union's Horizon 2020 research and innovation programme under grant agreement No 861950.

**AUTHOR**


| Author | Organization | Contact (e-mail, phone) |
|---|---|---|
| Nicolas Vogel | FAU | nicolas.vogel@fau.de |
| Vaibhav Gupta | FAU | vaibhav.gupta@fau.de |
| Stephan Suckow | AMO | suckow@amo.de |
| Javier Aizpurua | CSIC | jaizpurua@ehu.eus |
| Ruben Esteban | CSIC | ruben.esteban@ehu.eus |
| Jose Luis Montaño | CSIC | luismpriede@gmail.com |
| Jeremy Baumberg | UCAM | jjb12@cam.ac.uk |


**DOCUMENT DATA**

| | |
|---|---|
| Keywords | On-chip Quantum dot light source, Disc-on-disc nanoantenna, Colloidal lithography, Self-assembly, Colloidal Quantum dots, plasmonic |
| Point of Contact | Name: Nicolas Vogel<br>Partner: FAU<br>Address: Cauerstrasse 4, 91058 Erlangen<br>Phone: 09131 8520357<br>E-mail: nicolas.vogel@fau.de |

**DISTRIBUTION LIST**

| Date | Issue | Recipients |
|---|---|---|
| 17/01/2024 | V1.0 | EC & all partners through OwnCloud |

**REVIEW PROCESS**

| Document version | Date | Status/Change |
|---|---|---|
| V0.1 | 01/12/2023 | Draft discussion |
| V0.2 | 12/12/2023 | Complete draft |
| V0.3 | 21/12/2023 | Final version for review |
| V1.0 | 17/01/2024 | Final version |

**VALIDATION PROCESS**

| Reviewers | | Validation date |
|---|---|---|
| Work Package Leader | Nicolas Vogel (FAU) | 12/12/2023 |
| Project Coordinator | Stephan Suckow (AMO) | 17/01/2024 |

## Executive Summary

This report shows the way to successfully integrate optically pumped colloidal light sources within waveguide architectures directly on a chip. The approach involves the fabrication of suitable nanoantenna structures, the integration of colloidal quantum dots (QDs) while preserving their emission properties, and their integration within a cavity on a waveguide chip. First using theoretical inputs from WP1, disc-on-disc architectures were identified as promising nanoantenna structures. Arrays of such disc-on-disc structures are first fabricated on plain glass substrates to optimize their optical properties. Plasmonic resonances at 640 nm and 1550 nm were achieved. The location of QDs for maximum absorption and emission enhancement was determined by exploring different plasmonic resonance profiles based on angle dependent optical and near-field properties. In order to access the high E-field regions at the outer boundary of the dielectric spacer separating the two discs, we employed a controlled wet etching process to open a defined gap within this dielectric spacer layer. For 640 nm emission of CdS/CdSe QDs, larger gap openings were preferable due to the concentrated near-field at the disc center for the plasmonic resonance at this spectral range. Conversely, for 1550 nm emission QDs, the plasmonic resonance identified for emission enhancement had near-fields concentrated at the rim of the gap region. Thus, a smaller gap opening was preferred. Despite progress in 640 nm emission QDs, challenges persist in finding air-stable 1550 nm emission QDs.

The knowledge derived from our studies on glass substrates played a crucial role in guiding the parameters for the on-chip integration. For the targeted placement at the desired location, we introduced a sacrificial photoresist layer, which served two purposes. Firstly, it allowed depositing antenna structures at predefined spots of the chip via holes within the resist layer. Secondly, it allowed a simple removal of antennas that were not within the targeted area. This strategy enabled us to exclusively place the nanoantennas inside the cavities. We then deposited a layer of colloidal QDs onto the complete architecture. By means of capillary forces, QDs were placed within the opened gaps separating the two nanodisc structures, where, as we showed before, they experience a large near-field enhancement. This two-step strategy was chosen to separate the emitter integration from the actual fabrication process, thereby reducing damage to the QDs – and thus loss of emission properties - during fabrication. Together, the developed approach provided a complete pathway to integrate functional QDs within nanoantennas directly at the desired positions within a waveguide-containing chip. We subsequently demonstrated the ability of these nanoantennas to enhance the QD emission, and to couple this emission into the waveguide, as described in the deliverable of WP5.

# Table of contents



## Table of Figures

# 1. Introduction

The central goal of POSEIDON is to achieve an integrated photonic configuration where colloidal quantum dot (QD) emitters can efficiently emit light and their emission can be effectively coupled to a waveguide, providing a functional and integrated on-chip light source. To that end, one needs to enhance the efficiency of light emission from the QDs with the use of plasmonic antennas for light collection and near-field enhancement (Deliverable 3.1). These nanoantenna-emitter systems are subsequently integrated at predefined locations within a waveguide as on-chip light sources. Initially, we proposed to also develop epsilon zero (or near-zero) materials (ZIMs) to enhance and direct the light emission properties (Deliverable 3.2). During the project, the consortium followed the suggestion of the reviewers to critically assess the different approaches and focus on the most promising strategies towards the goal of on-chip integration. As a result, the development of ZIMs was discontinued, as detailed in the amendment to the consortium agreement. This decision was supported by the results presented in Deliverable 1.4, and validated by the reviewing panel, and thus, the research efforts shifted towards the direct integration of the QD-containing nanoantennas. A major challenge in these developments, as reported in the technical report M36, was the loss of emission properties of QDs, presumably by damage during fabrication. In this report, we present our approach to mitigate this challenge and allow a functional integration of emissive QDs within nanoantenna architectures. By decoupling the QD integration process from the fabrication steps, we avoid damage to the QDs, and thus preserve their emission properties upon integration within a waveguide structure.

The strategy for the design of colloidal light sources was established as follows.
First, we used disc-on-disc nanoantennas as plasmonic architectures for emission enhancement, following an evaluation of enhancement efficiency (guided by simulations, see results in WP1 (Deliverable 1.4), and in WP3 (Deliverable 3.1), and the ability for reliable fabrication and integration within the device.
Disc-on-disc nanoantennas consist of two gold nanodiscs separated by a silicon dioxide spacer layer. We used colloidal lithography to produce these architectures and explored their plasmonic properties as a function of disc size and spacer thickness. Subsequently, we partially dissolved the silicon dioxide dielectric layer through a wet-chemical etching process using a basic aqueous solution. Notably, this etching process affords control over the gap opening within the layer as the etching proceeds from the outer region towards its center. Subsequently, we conducted an analysis of the optical resonances of the disc-on-disc nanoantenna array under different angles of incidence, for both etched and non-etched cases. Additionally, we examined the simulated near electric field (E-field) profiles for both etched and non-etched nanoantennas across all the studied plasmonic resonances. This detailed characterization informed the choice of plasmonic antenna parameters, respective location of QD with the nanoantenna and angle of excitation to achieve emission enhancement. As a last step, we integrated the colloidal QD light sources into the nanoantennas. Separating these integration step from the actual nanoantenna fabrication ensured that the emission profile of the colloidal QDs remains intact. We leveraged capillary forces acting on the colloidal particles upon drying to position QDs within the opened cavity. To achieve plasmon-enhanced light emission, it is crucial to ensure the precise alignment of both the structural and optical properties of the two components. Firstly, the position of the emitter within the cavity must be controlled to prevent quenching while simultaneously providing a high E-field enhancement. Secondly, the excitation of the emitter should be spectrally matched with the response of the plasmonic resonance to maximize the excitation enhancement. Finally, if the emission wavelength of the emitter coincides with the prevailing scattering resonance of the cavity, it can lead to alterations in emission properties through the Purcell enhancement. Finally, the nanoantenna is used to impart directionality in the far-field QD emission.

With all this understanding we finally integrated the disc-on-disc nanoantenna on-chip with waveguide architectures using a combination of bottom-up and top-down processing, as detailed in this report.

# 2. Realization disc-on-disc nanoantenna on glass substrate

## 2.1. Fabrication of disc-on-disc nanoantenna on glass substrate

We utilize colloidal lithography[1] as an experimentally simple and parallel method for generating arrays of disc-on-disc nanoantennas. The fabrication process, outlined in Figure 1A, starts with the deposition of thin films of gold, silicon dioxide, and gold on a glass substrate through thermal evaporation. Subsequently, a monolayer of polystyrene colloidal particles, previously preassembled at the air/water interface,[2] is transferred onto the substrate. These polystyrene particles are then reduced in size via isotropic oxygen plasma treatment to open up space in between the different particles, which form a non-close packed arrangement after etching.[2] Next, a directed reactive ion etching process, oriented perpendicular to the surface, is employed to selectively remove any material not protected by the particles. This step removes parts of the gold and silicon dioxide layers not shielded by the shadowing effect of individual particles. As a result, circular patches of the sandwiched layers result. Following the removal of the colloidal mask using adhesive tape, an array of disc-on-disc nanoantenna structures is formed on the substrate (Figure 1B).

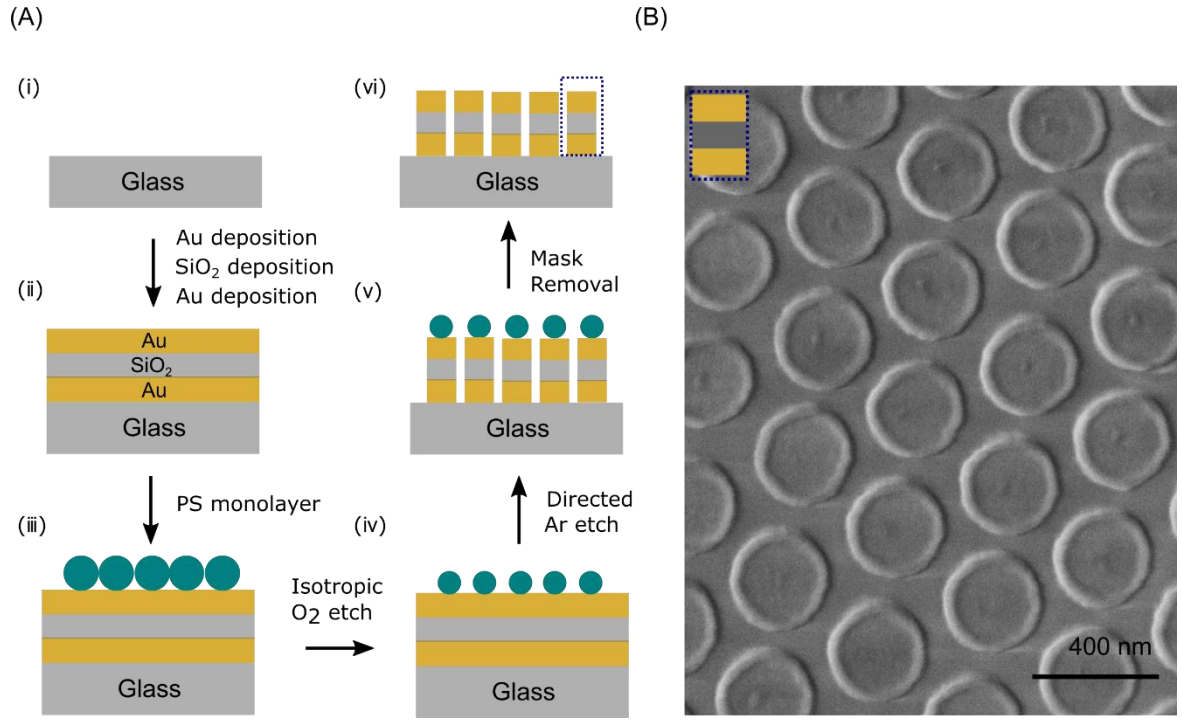


***Figure 1**: **Fabrication of disc-on-disc nanoantenna on glass substrate**: (A) The fabrication process illustrated schematically, encompassing sequential depositions of gold, silicon dioxide, and gold thin films on a substrate (ii). A colloidal monolayer is then applied to the substrate (iii) and reduced in size through oxygen plasma treatment (iv). A directed Argon-ion etching process selectively eliminates material not protected by templating particles (v), ultimately resulting in the formation of a disc-on-disc nanoantenna array after the particles are removed (vi). (B) Scanning electron microscope (SEM) image of the disc-on-disc array where the inset shows the thickness of individual building blocks.*

## 2.2. Optical Properties of the disc-on-disc nanoantenna array

We proceeded by submerging the disc-on-disc nanoantennas in a sodium hydroxide (NaOH) solution with varying concentrations to selectively remove parts of the silicon dioxide spacer layer that separates the gold nanodiscs. Figure 2A displays schematic illustrations of both non-etched and etched disc-on-disc arrays, which were immersed in low and high concentrations of aqueous NaOH.

We characterize next the optical properties of these disc-on-disc nanoantenna by analyzing the optical absorbance A under transverse magnetic (TM) polarization and changing the angle of incidence from 0° (normal to the surface) to 60°. The absorbance is defined as $\mathbf{A} = -\boldsymbol{log}\ (\mathbf{T})$, where $T = I/I_0$ is the transmission coefficient, $I_0$ the incident intensity and I the simulated transmitted intensity. Figure 2B compares the experimental (left panel) and simulated (right panel) absorbance. For this comparison, the simulations

consider a hexagonal array of double-disc nanoantennas in an Au-$SiO_2$-Au configuration supported on a glass substrate. Crucially, the measured spectra reveal a series of resonant peaks that are generally in very satisfactory agreement with the simulated results, appearing at similar wavelengths and showing the same trends with angle of incidence and etching. The main difference is that the peaks at lower wavelengths (≈600-800 nm) are considerably broader in the measured than in the simulated spectra, which can be attributed to increased losses in the experiments due to fabrication imperfections (rugosity, differences between different double discs antennas, non-perfect periodicity).

More in detail, the experimental absorbance spectra of the non-etched structures under normal incidence illumination reveal two plasmonic resonances at ≈780 nm and ≈1320 nm (left panel in Figure 2B, angle of incidence = 0º), with corresponding peaks appearing in the simulations at similar wavelengths (≈660 nm and ≈1400 nm) (right panel). As the incidence angle is increased, the peak at larger wavelength remains relatively unchanged in both simulations and experiments. In contrast, the peak at lower wavelength splits into two different peaks for large angles of incidence. The wavelength of the maxima of these peaks redshifts with increasing angle. This behavior is the consequence of localized plasmonic modes (i.e., resonances that are associated with each individual disc-on-disc nanoantenna) and grating modes introduced by the hexagonal periodicity of the sample. The grating modes are characterized by a strong dispersion with angle of incidence. On other hand, the localized plasmonic modes of the double disc structure can be understood in the following way: each thin disc supports a plasmonic surface wave that propagates along the disk until it is reflected at the edges, giving rise to Fabry-Pérot resonances when constructive interferences between the different reflected waves occur. The Fabry-Pérot modes of one of the discs will couple with those of the other, leading to hybridized resonances that can increase light concentration in the gap between them (when the fields at the gap dominate the response, an equivalent picture describe the Fabry-Pérot modes based on the plasmons excited at the metal-insulator-metal configuration forming the gap). The frequency of these localized modes does not depend on the angle of incidence, but modes that cannot be excited at normal incidence (due to symmetry) becomes accessible for oblique incidence. Importantly, the plasmonic and grating modes interact, which leads to a complex resonant behavior including possible mode hybridization. Simulations of the optical response of isolated double-disk nanoantennas was also performed (not shown here).

Additionally, upon subjecting the arrays to the etching procedure, the main effect is a blue shift of most peaks in the experimental and in the simulated spectra (compare solid and dashed lines before and after etching, respectively). This spectral shift is due to the reduction in the effective refractive index ensuing from the removal of silicon dioxide of the spacer layer and supports the successful removal of the dielectric spacer material at the outer parts of the double-disc nanoantenna. The blue shift is significantly more marked for the peak at lower wavelengths, due to the spatial distribution of the associated electromagnetic fields, as discussed in more detail below.

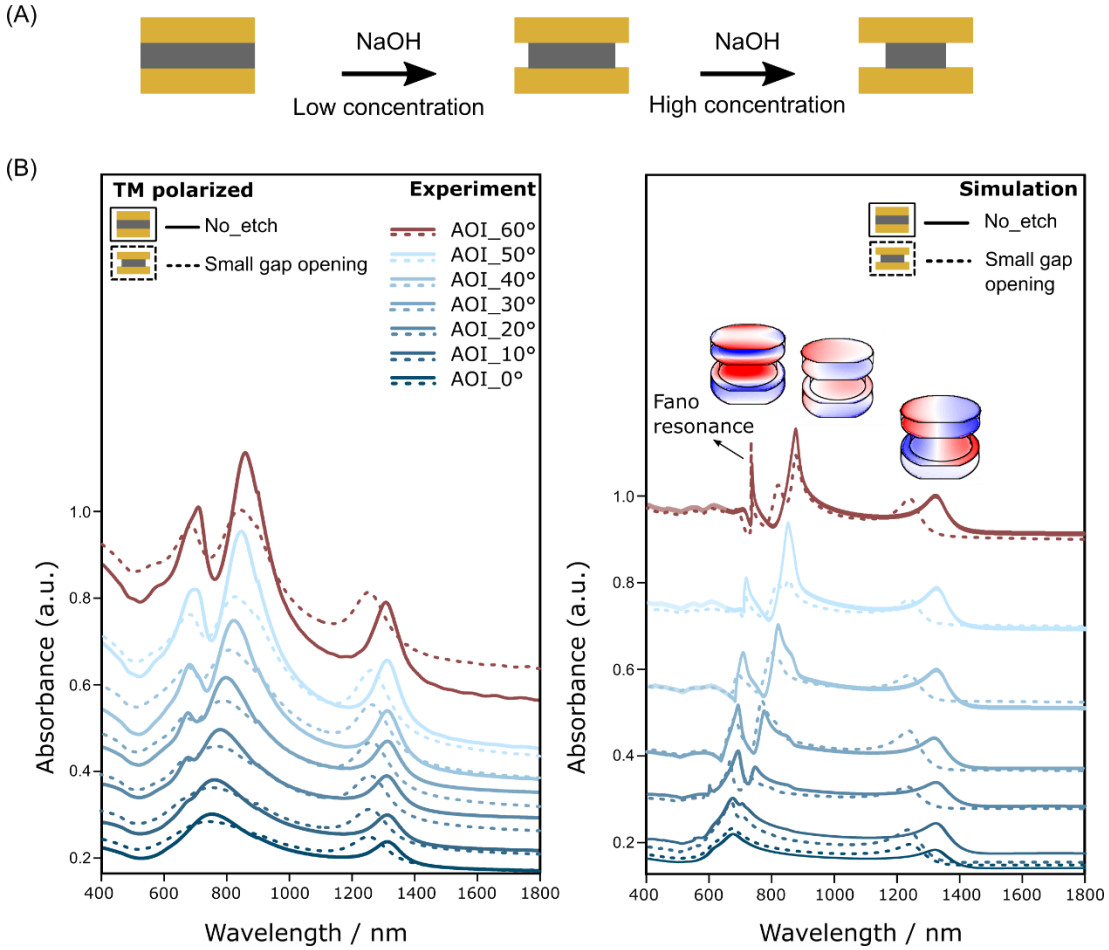


***Figure 2: Optical properties of disc-on-disc nanoantenna array:*** *(A) Schematic illustration of the structural change in disc-on-disc nanoantennas due to exposure to low and high concentrations of NaOH. (B, left panel) Absorbance spectra for non-etched (solid lines) and 0.4 M etched (dashed lines) disc-on-disc nanoantenna arrays under TM excitation. (B, right panel) Calculated absorbance spectra ($A = -log\ (T)$) of disc-on-disc nanoantennas placed in a hexagonal array with lattice parameter 380 nm and supported on a glass substrate. In both panels, the spectra are shown for different angle of incidence and shifted vertically for better readability (normal incidence, corresponding to angle of incidence = 0°, at the bottom, and angle of incidence = 60° at top). The insets in (B, right panel) show the calculated charge distributions at the four circular surfaces of the two gold discs, obtained at the frequencies of the three resonant peaks after etching, when angle of incidence = 60°.*

## 2.3. Simulation based near E-field profile

To complement the analysis of the optical properties of the system, maps of the spatial distribution of the electric field enhancement are simulated and shown in Figure 3 for illumination at angle of incidence = 60º and at the wavelength of the three peaks in the corresponding spectra ($\lambda_1$ = 733 nm, $\lambda_2$ = 875 nm, and $\lambda_3$=1240 nm). The structure with a reduced diameter of the $SiO_2$ spacer is considered in this case to include the effect of etching (the associated charge distribution is shown in the inset of Figure 2B). The local electric field is enhanced up to a factor ≈10 for the illumination at $\lambda_1$ = 733 nm and $\lambda_3$=1240 nm, that would correspond to ≈100 enhancement of the excitation rate (or of the radiative emission rate) for an emitter situated at the position of maximum fields. Further, the fields excited at $\lambda_1$ = 733 nm (Figure 3, left column) are maximum at the center of the disc and roughly exhibit rotational symmetry. In contrast, the field distribution is very different for $\lambda_3$=1240 nm (right column), with the maximum field enhancement near the edges of the gap. This field distribution corresponds to the excitation of (interacting) dipolar modes of opposite orientation at each of the two gold discs. Last, the field enhancement under $\lambda_2$ = 875 nm excitation is strongest around the top edges of the upper gold disc up to a factor ≈4 (corresponding to ≈16 enhancement of the excitation rate).

These results indicate that the three resonances can enhance the emitted signal, but that excitation at $\lambda_3$=1240 nm is particular promising due to the strong field enhancement at a region where the QDs will be deposited according to the fabrication procedure described in section 2.4. The localized plasmonic resonances can be tuned by changing size and thickness of the discs (as studied in detail in WP1, see Deliverable 1.4), making it possible to adapt the response of the double disc array to the absorption and emission frequency of different QDs. The spatial distribution of the fields excited at $\lambda_3$=1240 nm also explains the larger shift experienced by this mode after etching the sample (Figure 2). The resonant wavelength of a plasmonic resonance is particularly sensitive to changes of the refractive index in regions characterized by strong field enhancement, and the etching procedure removes the $SiO_2$ spacer at the gap edge, where the fields excited at $\lambda_3$=1240 nm are enhanced more efficiently.

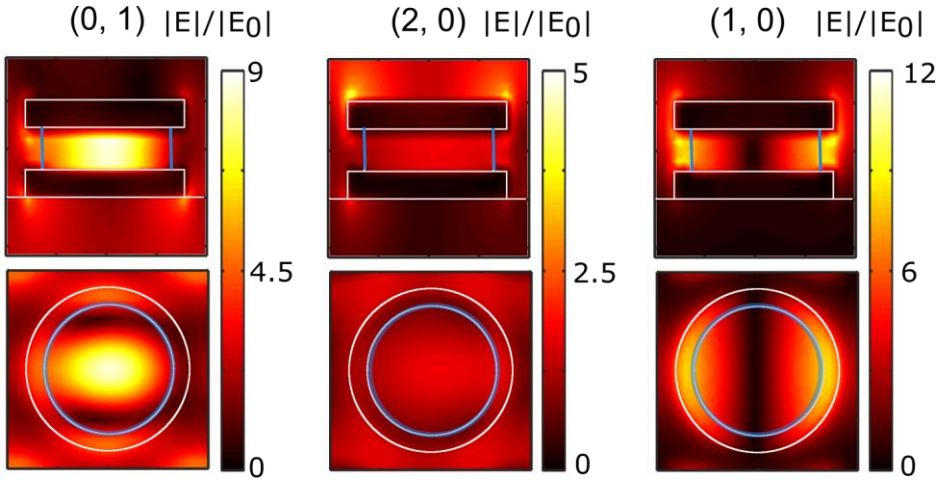


***Figure 3: Electric field maps for etched double-disc nanoantenna arrays.*** *Simulated spatial distribution of the amplitude of the electric field enhancement ($|E/E_0|$; $E_0$ electric field amplitude of the exciting plane wave) obtained at vertical (upper maps) and horizontal (bottom maps) planes going through the centre of the gap. The simulations consider the etched double-disc nanoantenna hexagonal array described in Figure 2, excited at the wavelength of the resonant peaks for angle of incidence = 60°. These wavelengths are indicated at the top of the figure (left column $\lambda_1$ = 733 nm, central column $\lambda_2$ = 875 nm, right column $\lambda_3$=1240 nm). Metal boundaries are outlined by a white line, and dielectric boundaries by a blue line.*

## 2.4. Integration of colloidal QDs into the nanoantenna structure

To probe the efficiency of the disc-on-disc nanoantennas in enhancing the light emission of colloidal QDs, we integrate lead sulfide (PbS) QDs into the preformed disc-on-disc nanoantennas. We selected PbS QDs with an emission wavelength of 900 nm to match the emission properties with the plasmonic resonance of the nanoantenna at $\lambda_2$ (see Figure 3). For this integration step, a two-dimensional array of PbS QDs (typically referred to as QD monolayer) was pre-assembled at a liquid interface by spreading a solution of PbS QDs dispersed in hexane at the air/diethylene-glycol interface, as depicted in Figure 4A.[3] Subsequently, the QDs were deposited onto solid substrates with the preformed disc-on-disc nanoantenna arrays. This approach enables a direct comparison of emission properties across different nanoantenna structures, as all solid substrates are decorated with the same number of QDs (i.e. a two-dimensional, uniform layer). We compared four distinct samples, as shown in Figure 4B: a continuous gold film as a reference, a non-etched disc-on-disc array with the gap that is completely filled with the silicon dioxide dielectric, a low concentration NaOH etched disc-on-disc array with a small gap opening, and a high concentration NaOH etched disc-on-disc array with a larger gap opening. Notably, in the case of the gold film, a significant portion of QDs is quenched, whereas the high concentration NaOH etched case demonstrates a remarkable 9-fold increase in photoluminescence intensity compared to the gold reference (Figure 4C).

Importantly, when a thin liquid film dries on a structured surface, capillary forces drag the meniscus into small structural features.[4] This mechanism in our case serves as an efficient tool to drag the QDs into the small gap opening provided in the etched samples. We uniformly excited all structures using a 633 nm laser, closely matching the nanoantenna resonance at the lowest resonant wavelength in Figure 2B

($\lambda_1$=733 nm at angle of incidence = 60º), which exhibited a high near-field at the center of the disc, as depicted in Figure 3. This configuration provides absorption enhancement with an increased gap opening (etching concentration). Consequently, we achieved more absorption enhancement in the etching with high NaOH concentration case due to a larger gap opening, where more QDs are drawn into the high field enhancement regions. Compared to the non-etched samples, this increased accessibility of the hotspot region increased the emitted light intensity by a factor of ~9. The electric field profile at the resonance of $\lambda_2$=875 nm in Figure 3 illustrates that the majority of the increase of the radiative enhancement originates from the QDs located at the rim of the top metal disc, as most of the field enhancement is concentrated in that region.

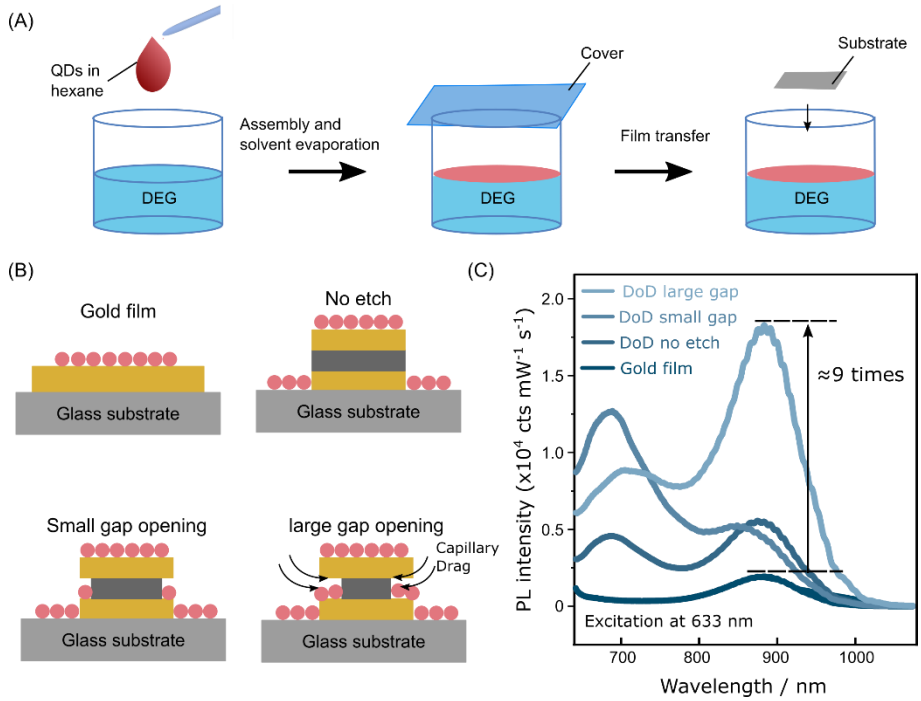


***Figure 4: Photoluminescence enhancement of PbS QDs in etched disc-on-disc nanoantenna:*** *(A) Self-assembly of PbS QDs into a two-dimensional layer, using a liquid interface (air/diethylene-glycol). (B) Transfer of the preformed QD monolayer onto various substrates and nanostructures. (C) Photoluminescence intensity spectra of the QDs deposited on various substrates.*

# 3. Fabrication of disc-on-disc nanoantenna light source on-chip

## 3.1. Fabrication process for the selective placement of nanoantenna architectures at predefined locations of the device

Figure 5 schematically illustrates the process for the on-chip integration of the disc-on-disc nanoantennas coupled with QDs which are exclusively positioned within a cavity in front of the waveguide. For this integration, the waveguide device was modified as follows: a cavity was integrated in front of the silicon nitride (SiN) waveguide, into which the nanoantenna can be integrated. The entire device was covered with a photoresist layer to protect the surface, except for the cavity as the designated area for the nanoantenna integration. Figure 5a schematically shows this architecture.

We subsequently implement the nanoantenna fabrication directly on-chip, as illustrated in Figure 5ii-v. Thin films of gold, silicon dioxide, and gold were deposited sequentially on the chip. These thin films serve as the foundation upon which the nanoantenna structures will be fabricated. A monolayer of preassembled polystyrene particles, initially formed at the air/water interface, is transferred to the substrate as shown in Figure 5 (iii). The particle size is subsequently reduced through isotropic oxygen plasma treatment, promoting a non-close packed arrangement. Utilizing directed reactive ion etching perpendicular to the

surface, material not shielded by particles is selectively removed. Upon removal of the colloidal mask, an array of disc-on-disc nanoantenna structures is obtained (Figure 4 (iv)). At this stage, the nanoantenna structures are formed homogeneously throughout the device, both inside the cavity and on the areas covered by photoresist. Subsequently, the substrate is immersed in an NaOH solution, followed by immersion in tetrahydrofuran (THF) solvent for an additional 2 minutes and a final rinse with water. This treatment removes the protective photoresist layer, and, along with it, the disc-on-disc nanoantenna from all regions of the substrate covered by it. In addition, the NaOH treatment causes etching of the spacer layer separating the disc-on-disc nanoantennas that remain within the cavity, as depicted in Figure 4 (v). As a final step, we deposit a layer of colloidal QDs (cadmium sulfide core / cadmium selenide shell (CdS/CdSe) for operation in the visible range), pre-assembled on an air- diethylene-glycol (DEG) interface onto the device.[5,6] Within the cavity, the QD layers are deposited onto the disc-on-disc nanoantennas, where capillary forces drag individual QDs to the region of high near field intensity within the gap opening (Figure 4vi). Additional QDs deposited onto the device outside the designated area at the cavity are currently removed by an adhesive tape, a step that could be integrated into the photoresist removal step in the future.

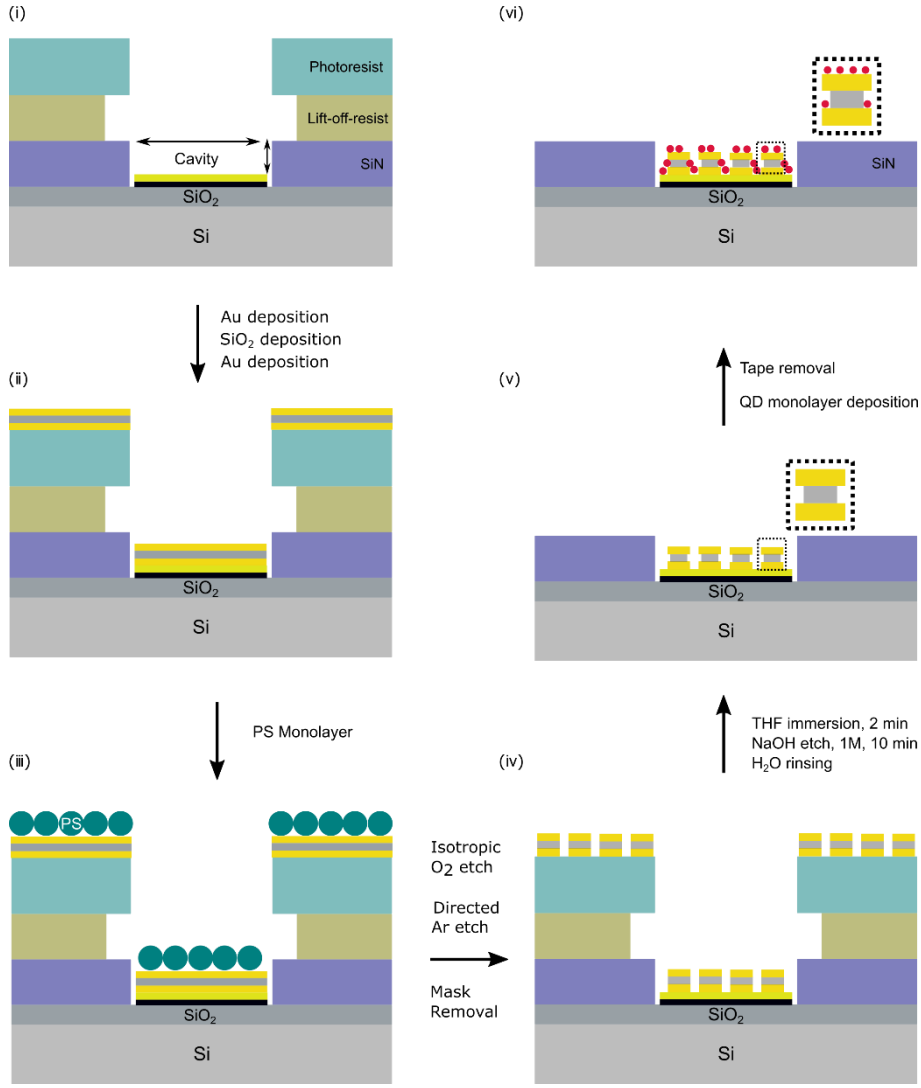


***Figure 5: Fabrication of on-chip disc-on-disc nanoantenna using colloidal QDs:*** *(i) A chip is shown with SiN waveguide architecture. (ii) Deposition of gold, silica, and gold layers, (iii) Monolayer assembly of PS particles, (iv) Size reduction of PS particles through oxygen plasma and Argon-ion etching, resulting in disc-on-disc nanoantenna on-chip, (v) THF immersion, NaOH etching, and $H_2O$ rinsing to achieve a reduced spacer diameter inside the cavity (boxed), (vi) Monolayer pre-assembly and placement of CdS/CdSe core-shell QDs, leading to exclusive localization within the cavity after tape removal (vi).*

## 3.2. Structure characterization of the disc-on-disc nanoantenna on-chip with CdS/CdSe QDs

Figure 6A shows an optical microscope image of the waveguide-containing chip after the localized placement of disc-on-disc nanoantennas at the predefined cavities, before the incorporation of QDs, akin to Figure 5v. The image highlights five distinct cavities, each possessing a fixed cavity length of 10 µm and

varying widths of 5 µm, 4 µm, 3 µm, 2 µm, and 1 µm from left to right. In the upper region of Figure 6A, all cavities feature a bottom gold mirror as outlined with solid line rectangles. Conversely, the lower region of Figure 6A illustrates cavities without a bottom mirror, marked by dashed line rectangles. Furthermore, SEM images of these cavities are presented in Figure 6B, revealing a hexagonal arrangement of the etched disc-on-disc nanoantennas, which are exclusively found within the cavities. These representative images underline the precision with which the disc-on-disc nanoantennas are placed at the predefined location directly on-chip.

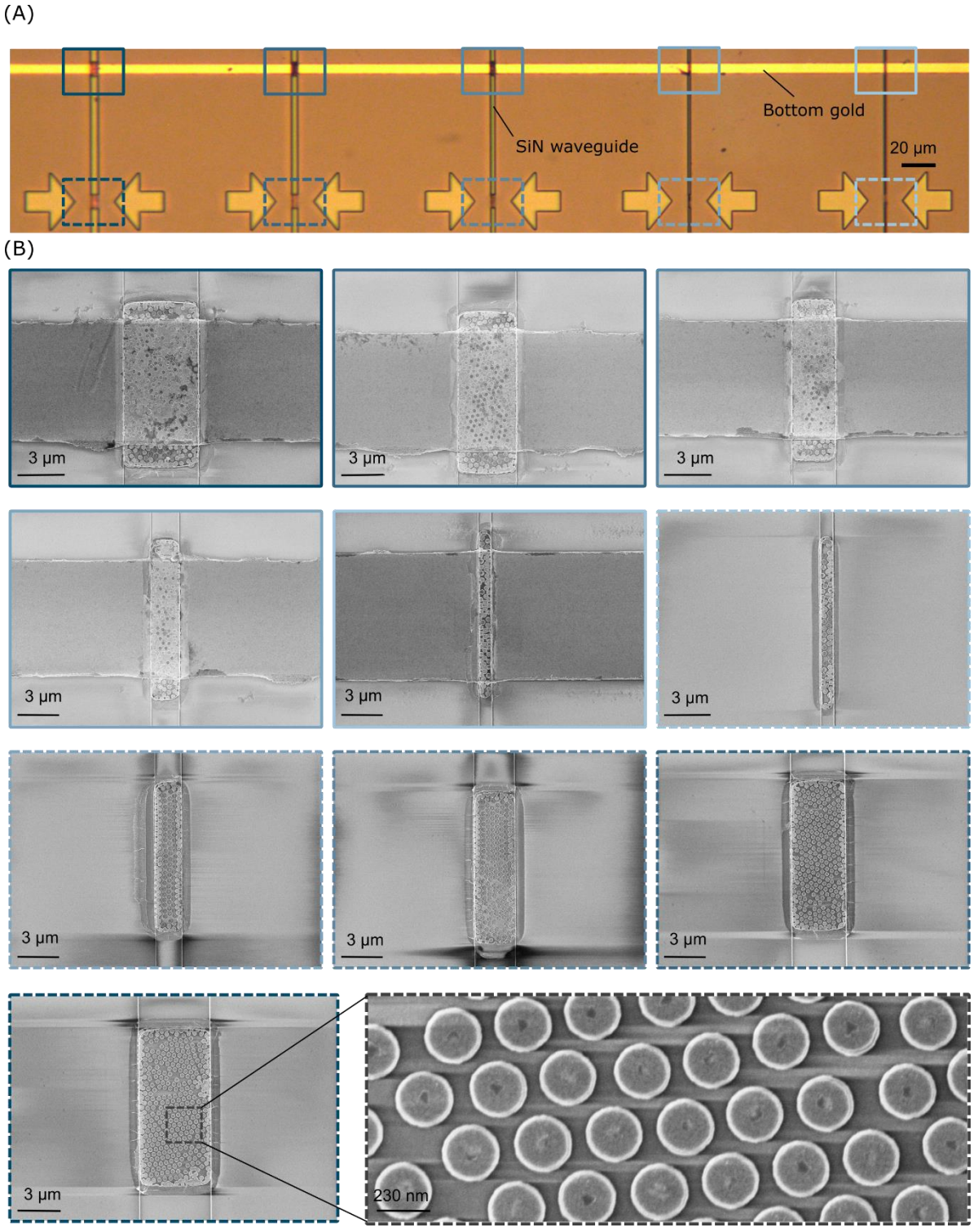


*Figure 6:* ***Surface characterization of the integrated waveguide chip decorated with disc-on-disc nanoantenna in designated cavities at the waveguide entrance:*** *(A) Optical microscope image of the chip, featuring etched disc-on-disc arrays within the cavities. The upper region highlights cavities with a bottom gold mirror (solid line boxes); the lower region features cavities without the bottom gold mirror (dashed line boxes). The cavity width decreases from left to right. (B) SEM images showing cavities of varying widths with and without the gold mirror, revealing a hexagonal arrangement of the disc-on-disc structure exclusively within the cavity.*

We next integrated a monolayer of CdS/CdSe QDs onto the nanoantenna-functionalized waveguide chip. In this case, we chose CdS/CdSe QDs with an emission wavelength of 640 nm as one of the target wavelengths in POSEIDON. As before, this QD layer was pre-assembled at the air-diethylene-glycol liquid interface and transferred directly to the chip as a solid substrate. Figure 7A shows dark field images with visible QD emission throughout the surface of the waveguide. In a proof of principle experiment, we removed undesired QDs from the waveguide surface by means of an adhesive tape. As the cavity is shielded from this procedure due to its lower height compared to the surrounding areas, the QDs deposited on the disc-on-disc nanoantenna arrays remained on the substrate, evidenced by the before (Figure 7A) and after (Figure 7B) tape removal dark field images from the cavities, shown for 5 µm and 3 µm cavities.

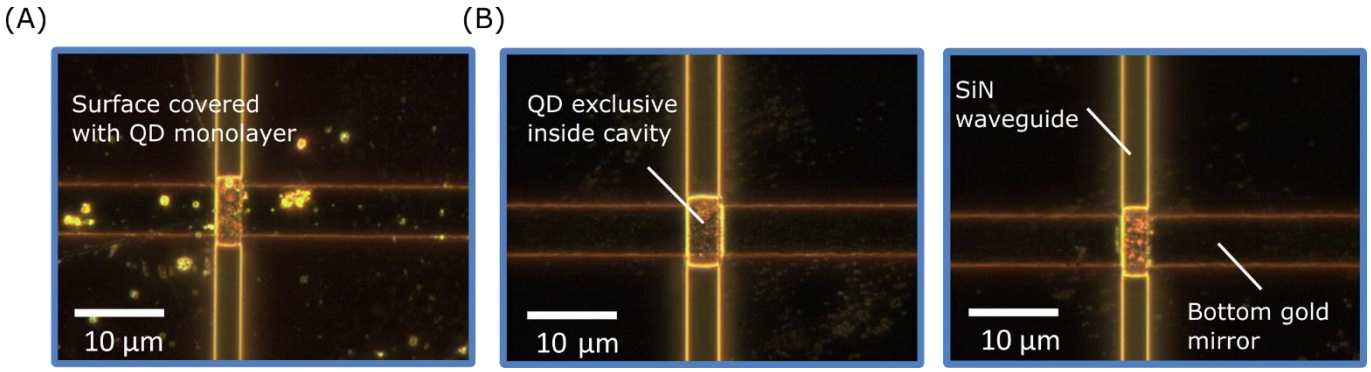


*Figure 7:* ***Integration of on-chip CdS/CdSe QDs into disc-on-disc nanoantenna arrays within a predefined cavity for waveguiding architectures:*** *(A) Optical microscope image of CdS/CdSe QDs assembled as a monolayer on the chip's surface. (B) Isolated QDs confined solely within cavities featuring etched disc-on-disc nanoantennas, achieved by selectively removing QDs from the flat surface using adhesive tape.*

### 3.3 Fabrication and characterization of disc-on-disc nanoantenna for telecom (1550 nm) wavelength

To target the second wavelength of interest in POSEIDON (1550nm), we redesigned the structure of the disc-on-disc nanoantennas to provide plasmonic resonances at 1550 nm. Leveraging our prior understanding of the near-field profile in such structures, we observed enhanced near-field intensity at the rim of the dielectric disc for the lowest energy plasmonic resonance as shown in Figure 3, which we targeted for emission enhancement at telecommunication wavelength. Consequently, we etched the dielectric silicon dioxide layer, with the intention of positioning the QDs directly at the gap opening where the near-field enhancement is largest (see Figure 3). To this end, the substrate was immersed in the NaOH solution, resulting in the etched disc-on-disc array on a model glass substrate as shown in Figure 8A. Further examination of the optical mode profile under TM polarization at various angle of incidences (0°, 30°, 45°, and 60°) revealed a plasmonic resonance exhibiting a peak at 1530 nm. This plasmonic resonance, identified as the lowest energy resonance, now appeared at the ideal spectral location to enhance QD emission rates (Figure 8B). We subsequently followed the on-chip integration strategy shown in Figure 5 to integrate these modified disc-on-disc nanoantennas into the waveguide architecture, again at the same predefined location in a cavity in front of the waveguide. Figure 8C shows SEM images of the fabricated on-chip structures. The integration of suitable QDs with emission profiles at 1550nm is currently ongoing.

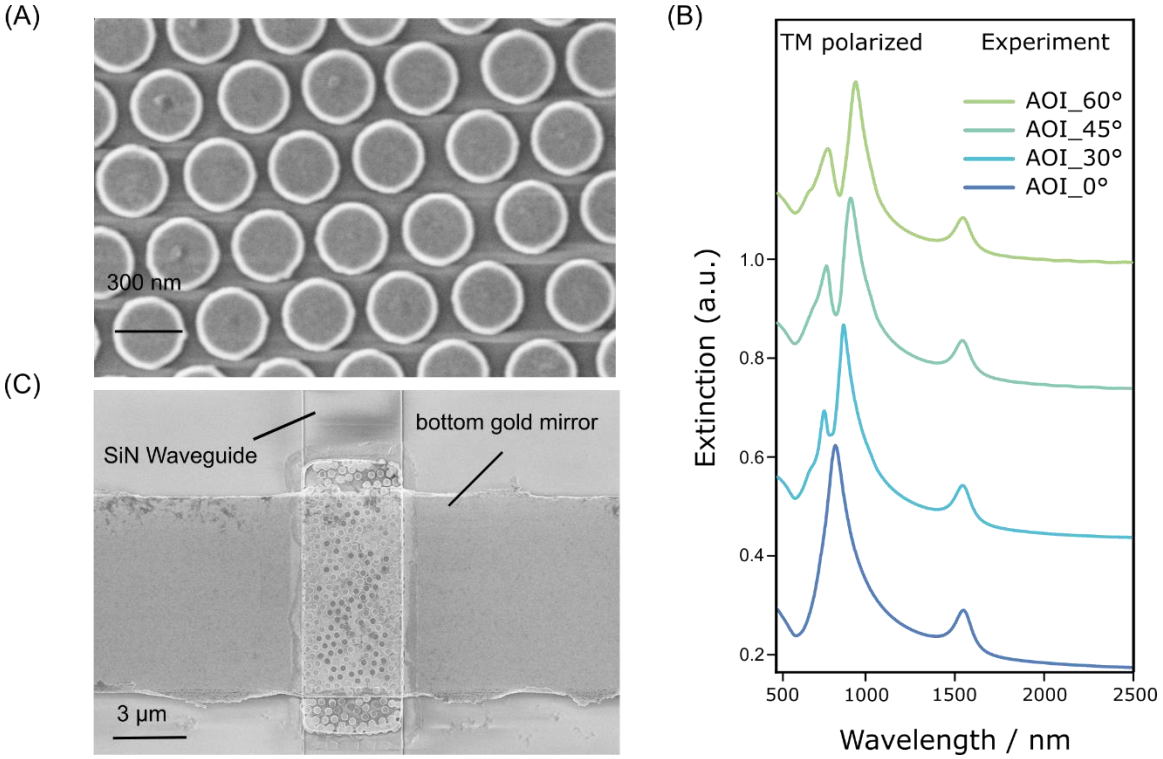


*Figure 8:* ***Fabrication, optical characterization, and on-chip integration of disc-on-disc nanoantennae for telecommunication wavelength emission at 1550 nm****: (A) SEM images of the etched disc-on-disc nanoantennae on glass substrate. (B) Extinction spectra of disc-on-disc nanoantenna array showing the resonance at the targeted spectral region of ~1550 nm. (C) SEM images of etched disc-on-disc nanoantennae integrated at the cavity of a waveguide chip.*

# 4. Conclusion

In conclusion, POSEIDON has demonstrated the successful integration of colloidal light sources within waveguide architectures. The produced architectures combine tailored nanoantenna designs with optimized nanoantenna-emitter configurations and demonstrated emission enhancement of integrated QDs of about one order of magnitude. This design was explored and optimized by computer simulations (see Deliverable 1.4 in WP1) and integrated into tailored waveguide-chips (WP5). The selective placement of such enhanced light sources is now available and serves as the basis for enhanced optical characterization, and successful coupling of light emission into waveguide modes (guided and rationalized by device-scale simulations, WP5), and potential electrical pumping (WP4).

Responding to constructive feedback from the reviewers, we redirected our research focus from ZIM integration to on-chip nanoantenna design using particle on mirror and disc-on-disc nanoantennas. As we outline in this document, this strategic decision enabled the technological breakthroughs targeted in POSEIDON. On a more technical level, we also addressed serious challenges related to QD degradation during fabrication, as reported in technical report M36. Our novel approach involves integrating QDs within the cavity of disc-on-disc nanoantennas in a two-step process to decouple the QD integration process from the nanoantenna fabrication.

Our methodology began with the fabrication of disc-on-disc nanoantenna arrays on glass substrates to understand their optical behavior, followed by on-chip integration. The design parameters for the disc-on-disc nanoantenna are guided by theoretical inputs from WP1 and WP5 to achieve targeted plasmonic resonances at 640 nm and 1550 nm. Among various parameters, we selected the dielectric spacer thickness as a crucial parameter for wavelength tuning. The complex plasmonic properties of the disc-on-disc nanoantennas, which exhibit multiple resonances that shift as a function of the angle of light incidence, enable a high degree of tunability and adaptability to the different targeted emission profile. A key innovation in the design of the disc-on-disc nanoantenna was the selective etching of the dielectric spacer layer, which allows opening regions with high near-field enhancement for QD deposition.

For 640 nm emission CdS/CdSe QDs, we established that the lowest wavelength resonance of disc-on-disc nanoantenna with a defined spacer thickness aligns with the emission wavelength, resulting in emission enhancement. Given that the near-field is concentrated at the center of the disc in this case, a larger gap opening achieved with a high concentration of NaOH were the preferred choice for fabrication. Conversely, for the 1550 nm emission QDs, the highest wavelength resonance of the nanoantenna matched the QD emission, promising emission rate enhancement. Considering that the near-field enhancement occurs at the rim of the dielectric in the resonance at 1550 nm, a smaller gap opening achieved with a reduced concentration of 0.4 M NaOH was preferred.

In our next step, we designed a chip for exclusive nanoantenna placement inside the cavity. Introducing a sacrificial photoresist layer streamlined the process and enabled the selective placement of the nanoantennas. The emissive QD layer can be subsequently integrated directly on chip via the deposition of a complete monolayer covering the entire surface. As a proof of principle, these QDs can be removed from unwanted regions of the chip simply via an adhesive tape. In the future, this step may be integrated in the photoresist removal step to streamline fabrication and make it more amendable to current nanofabrication processes. While the fabrication and integration steps are now established, finding suitable QDs with air stable emission at 1550 nm remains a challenge.

In summary, the POSEIDON project's innovative approach to on-chip design, nanoantenna integration, and QD incorporation within waveguide architectures holds promise for advancing integrated colloidal light sources, paving the way for applications in telecommunications and beyond. The achieved results not only contribute to the project's objectives but also provide valuable insights for the broader field of nanophotonics.

## 5. Literature

[1] N. Vogel, C. K. Weiss, K. Landfester, *Soft Matter* **2012**, *8*, 4044.

[2] N. Vogel, S. Goerres, K. Landfester, C. K. Weiss, *Macromol. Chem. Phys.* **2011**, *212*, 1719.

[3] A. Dong, J. Chen, P. M. Vora, J. M. Kikkawa, C. B. Murray, *Nature* **2010**, *466*, 474.

[4] S. Ni, J. Leemann, H. Wolf, L. Isa, *Faraday Discuss.* **2015**, *181*, 225.

[5] S. Hu, E. Elliott, A. Sánchez-Iglesias, J. Huang, C. Guo, Y. Hou, M. Kamp, E. S. A. Goerlitzer, K. Bedingfield, B. de Nijs, J. Peng, A. Demetriadou, L. M. Liz-Marzán, J. J. Baumberg, *Adv. Sci.* **2023**, *10*, 1.

[6] R. Chikkaraddy, B. de Nijs, F. Benz, S. J. Barrow, O. A. Scherman, E. Rosta, A. Demetriadou, P. Fox, O. Hess, J. J. Baumberg, *Nature* **2016**, *535*, 127.

## 6. Degree of progress

The deliverable is 100% fulfilled.

## 7. Dissemination level

Deliverable D3.3 is public.